

Performance of integrated thermopile vacuum sensors

A W van Herwaarden and P M Sarro

Department of Electrical Engineering, Delft University of Technology, PO Box 5031, 2600 GA Delft, The Netherlands

Received 7 March 1988, in final form 18 July 1988

Abstract. A quantitative insight is given into the performance of integrated thermopile vacuum sensors as a vacuum gauge. After a short résumé of their operation principle three pressure ranges are discussed. The zero repeatability is shown to be approximately 10 mPa. In the optimum pressure range of 1–100 Pa the error of prediction of the sensors is 2–3% while the upper pressure limit of the sensors is of the order of 5–50 kPa. Finally, a comparison with conventional Pirani gauges is made.

1. Introduction

In the last four years various thermal vacuum sensors based on integrated silicon thermopiles have been developed (Sarro and van Herwaarden 1986, van Herwaarden and Sarro 1987, 1988). For research objectives, one-dimensional models have been developed based on three characteristic parameters: the low-pressure sensitivity and two transition pressures. It has been shown that, with these models, the output signal of the sensor can be closely approximated on the basis of the pressure and three appropriate parameters.

In this paper a different approach is followed. The operation of the sensor as a vacuum gauge is examined, the pressure as predicted by the sensor output, to get an impression of the performance of the sensors as vacuum gauges (see figure 1, where the sensor output is given as the measured thermal conductance of the gas). By inserting the appropriate parameters and the sensor output into the one-dimensional model, the pressure can be calculated. This calculated pressure is then compared with the actual calibration pressure and the resulting differences, 'prediction errors', are an indication of the performance of the sensors as a vacuum gauge.

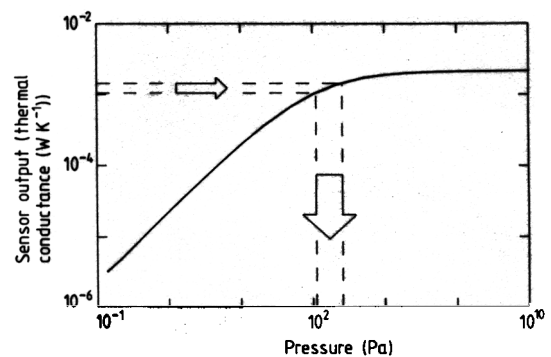


Figure 1. Output signal of a floating-membrane vacuum sensor plotted nitrogen pressure (expressed in the measured thermal conductance of the gas). Broken lines: output signal-to-pressure relation, indicating the increase in inaccuracy at high pressures due to the non-linearity of the sensor $G_0 = 1.94 \text{ W m}^{-2} \text{ K}^{-1} \text{ Pa}^{-1}$, $P_{t1} = 45 \text{ Pa}$, $P_{t2} = 142 \text{ Pa}$.

An essential difference exists between the prediction errors and the so-called 'simulation' or 'approximation' errors given in previous papers (van Herwaarden and Sarro 1987, 1988), in which the sensor output was calculated on the basis of the pressure and the three parameters. Due to the low sensitivity of the sensor at high pressures, going from pressure to sensor output results in only very small errors in the high-pressure region, see figure 1. In contrast to this, in normal operation as a vacuum gauge (the pressure being predicted by the sensor), a small variation in the sensor output results in a large (prediction) error in the predicted pressure, again because of the low sensitivity of the sensor at high pressures. This is made explicit by the broken lines of figure 1. To get a proper impression of the sensor performance as a vacuum gauge it is therefore necessary to study the prediction errors.

Below we will first give a short introduction to the operating principle and the one-dimensional models of the two thermal-vacuum-sensor types: the cantilever-beam structure and the floating-membrane structure. The performance of the sensors as a vacuum gauge is discussed in three parts: the low-pressure resolution; the mid-pressure range; and the high-pressure limit. Finally a comparison will be made with conventional Pirani gauges, on the basis of another paper (Poulter *et al* 1980) in which the reversed relation, pressure as a function of sensor output, has been studied.

2. Operating principle

2.1. Thermal conductivity of gases

The physical principle underlying thermal vacuum measurement is the pressure dependence of the thermal conductivity of gases. Let us consider the structure of figure 2, showing a hotplate suspended between two parallel heat sinks at distances M_1 and M_2 . If thermally conductive gas is present in this configuration the gas will transport heat from the hotplate to the heat sinks. The extent of this effect increases with increasing pressure as the amount of heat that can be conducted by the gas in the gaps is proportional to the number of gas molecules. However, when the mean free path between the collisions of the gas molecules becomes smaller than the gap size M_1 or M_2 , the thermal conductivity of the gas layer is no longer proportional to pressure. In this condition, if the number of molecules available for transferring heat is doubled, the effective distance over which they can carry the heat is halved. This results in a stabilisation of the thermal conductivity of the gas. In the situation of figure 2 the total thermal conductance G (in $\text{W m}^{-2} \text{K}^{-1}$) can be written as (Dushman

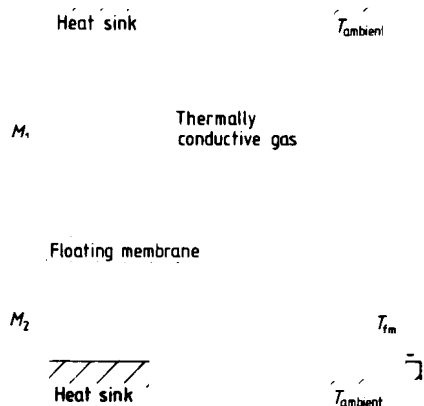


Figure 2. Cross section of the structure of the integrated thermal vacuum sensor mounted in a housing (not to scale).

1962, van Herwaarden and Sarro 1987)

$$G = G_0 P \left(\frac{1}{2} \frac{P_{11}}{P + P_{11}} + \frac{1}{2} \frac{P_{12}}{P + P_{12}} \right) \quad (1)$$

in which G_0 (in $\text{W m}^{-2} \text{K}^{-1} \text{Pa}^{-1}$) is the low-pressure thermal conductance of the gas around the sensor actually measured, G_0 is the pressure-independent constant, P represents the pressure dependence, while the expression between the brackets represents the stabilisation of the thermal conductance at high pressures. P_{11} and P_{12} are the transition pressures for the heat transfer in the widest gap and the smallest gap respectively, around which the thermal conductivity of the gas layer changes from being proportional to pressure to being independent of pressure. They are inversely proportional to the values of M_1 and M_2 , and for the typical dimensions of $M_1 \approx 0.9 \text{ mm}$ and $M_2 \approx 0.3 \text{ mm}$ it is found that $P_{11} \approx 50 \text{ Pa}$ and $P_{12} \approx 150 \text{ Pa}$. The resulting thermal conductance G can be seen in figure 1 for $G_0 = 1.9 \text{ W m}^{-2} \text{K}^{-1} \text{Pa}^{-1}$, $P_{11} = 45 \text{ Pa}$, $P_{12} = 142 \text{ Pa}$, and a hotplate area $B = 12 \times 10^{-6} \text{ m}^2$ (1 Torr = 133.32 Pa; atmospheric pressure is 100 kPa, 760 Torr). Two structures have been made to exploit the pressure dependence of the thermal conductivity of gases, a cantilever-beam structure and a floating-membrane structure, see figure 3. A completed sensor consists of a sensor chip such as those shown in figure 3, mounted in a standard ceramic IC housing with a cover on top. This results in the structure shown in figure 2, in which the bottom heat sink represents the bottom of the housing and the top heat sink represents the cover on top of the housing.

2.2. Convection

As well as the pressure dependence of the thermal conductivity of gases, convection is another physical principle that can be exploited to measure the absolute pressure of gases, especially at high pressures. Free convection occurs when temperature differences cause variations in the specific density of the gas. Consider figure 2. If gas is heated by the hot floating membrane, it will expand and start to move upwards, carrying heat away from the hot floating membrane. The warmed gas is replaced by cold gas, which in turn will be warmed up and carry some heat away. This process of heat transfer is called free convection, and the extent of this effect is proportional to the square root of the pressure. Free convection is often used in Pirani gauges to increase the upper pressure limit into the pressure range where the gas has viscous properties, and this has led to the development of gauges with atmospheric upper pressure limits (Steckelmacher 1973). However, free convection does not take place in small cavities, and for geometries like the integrated vacuum sensors described in this paper convection (theoretically) occurs only if gaps of more than 10 mm exist between the floating membrane and the heat sinks. This is never the case, which is why free convection has never been observed during any measurement. We will therefore not discuss this effect any further.

2.3. Cantilever-beam sensor

The cantilever-beam sensor operates in a constant-power measurement mode. In a heating resistor at the tip of the beam a constant heating power P_h is dissipated, resulting in a temperature increase of the tip of the beam with respect to its thermally grounded base. A thermopile of sensitivity $N\alpha_s$ measures the temperature difference between the tip and base of the beam (N is the number of thermocouples, with a Seebeck coefficient α_s , $N\alpha_s$ is typically $10\text{--}20 \text{ mV K}^{-1}$). The beam has a length L , a width W and a thermal sheet

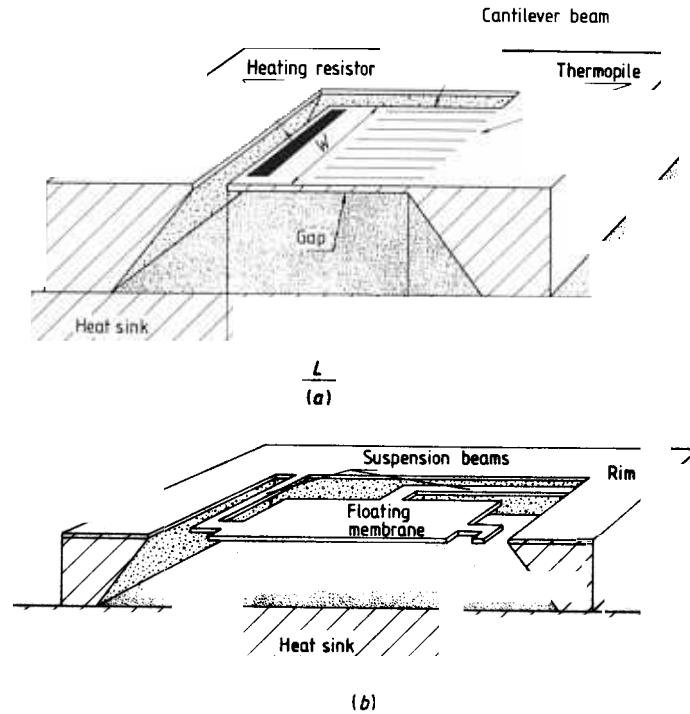


Figure 3. (a) Cross section of an integrated cantilever-beam vacuum sensor (not to scale). (b) Cross section of an integrated floating-membrane vacuum sensor with two of the four suspension beams visible (not to scale).

resistance R_{st} (L is typically 1–10 mm, W is typically 1–3 mm, and $R_{st} = 700 \text{ K W}^{-1} \square^{-1}$).

In the presence of a thermally conductive gas the beam will be cooled and the resulting thermopile output voltage U_{tp} as a function of the thermal conductance of the gas is given by (van Herwaarden and Sarro 1987):

$$U_{tp} = N\alpha_s R_{st} P_b \frac{L}{W} \left(\frac{\tanh \gamma L}{\gamma L} \right) \quad (2)$$

in which $\gamma^2 = GR_{st}$, with G as given by equation (1). For low pressures, where $\gamma L \ll 1$, equation (2) simplifies to:

$$U_{tp} = N\alpha_s R_{st} P_b \frac{L}{3W} (1 - \frac{1}{3} GR_{st} L^2) \quad (3)$$

During the experiments U_{tp} was typically 100 mV for zero G . For the analysis the output signal is normalised to this zero-pressure offset $N\alpha_s R_{st} P_b L/W$. Further, because we are interested in the pressure-dependent signal, only the deviation of the sensor output from the zero-pressure offset will be considered leaving us with the normalised decrease from the zero-pressure value $V(P)$:

$$V(P) = 1 - \frac{\tanh \gamma L}{(\gamma L)} \quad (4)$$

in which $V(P)$ is a function of the pressure P . For low pressures, where $\gamma L \ll 1$, equation (4) simplifies to:

$$V(P) = \frac{1}{3} GR_{st} L^2. \quad (5)$$

2.4. Floating-membrane sensor

The floating membrane is operated in a constant-temperature measurement mode. The constant-temperature mode is more difficult to implement than the constant-power mode used for the cantilever-beam sensors because it requires a feedback loop. It has the advantage, however, in that it results in an output signal directly proportional to the thermal conductance of the gas G (unfortunately, in the cantilever-beam

sensor such a simple relationship between G and the output signal cannot be obtained).

The floating-membrane sensor consists of a hotplate (the 'floating membrane') suspended between two parallel heat sinks by four small beams of high thermal resistance. Thermopiles in the suspension beams measure the temperature elevation T_{fm} (typically 10 K) of the floating membrane.

In the presence of thermally conductive gas this temperature elevation is kept constant by dissipating a heating power P_{fm} in a heating resistor which almost entirely covers the floating membrane, thus supplying the heat carried off by the gas (van Herwaarden and Sarro 1988):

$$P_{fm} = T_{fm} B G \quad (6)$$

In equation (6) B is the area of the floating membrane ($B = 12 \times 10^{-6} \text{ m}^2$), and G is once again given by equation (1). Note that the output signal P_{fm} is now directly proportional to the thermal conductance of the gas G , unlike U_{tp} for cantilever beams in equations (2) or (4). Since both T_{fm} (via the thermopile output) and B are known, the sensor output may also be given as $G (= P_{fm}/BT_{fm})$, the thermal conductance of the gas, see figure 1.

3. Pressure prediction

The output of the sensors as given by equations (4) and (6) is completely determined by three characteristic parameters. The first two are the transition pressures of equation (1), while the third is the low-pressure sensitivity. For a cantilever-beam sensor the low-pressure sensitivity is the factor $\frac{1}{3} G_0 R_{st} L^2$ of equation (5), while for a floating-membrane sensor it is simply $B G_0$. Here we will analyse how well the sensors can predict pressure using the model based on the three characteristic parameters. The strict adherence to this model may lead to somewhat larger errors, compared to simply calibrating the sensor and putting the calibration data in a ROM look-up table. In general, however, both the low-pressure sensitivity and the transition pressures are

different for different gases and, in addition, they depend upon temperature. An important advantage of using our model is, therefore, that it enables a correction for gas type and for ambient temperature when calculating the pressure, through adaptation of the characteristic parameters.

The analysis is as follows. First, the sensor is calibrated with a reference gauge. Then the characteristic parameters are estimated from (three of) the calibration points. Finally, the performance of the sensor is tested by inserting the three characteristic parameters and the sensor output into equation (4) or (6), predicting (albeit afterwards) the pressure with these equations and comparing the predicted pressure with the actual calibration pressure.

The equipment used for the calibrations consisted of a glass bell-jar in which the sensors were mounted, and to which a rotation and a diffusion pump were attached. A needle valve attached to the bell-jar allowed the introduction of small amounts of gas, and two Baratron capacitance manometers were used as reference gauges. The base pressure of the system was less than 3 mPa. In the low- and mid-pressure ranges a Baratron 227A capacitance gauge was used as reference, with a calibrated error of approximately 3% at 0.1 Pa, falling to less than 0.15% at pressures between 1 Pa and 100 kPa. In the high-pressure range from 100 Pa to 100 kPa a Baratron 222B was used as a reference, with a calibrated error of approximately 3% at 200 Pa, falling to less than 0.15% above 2 kPa.

Below we will examine the accuracy with which the sensors can predict the pressure on the basis of the sensor output and the three parameters for three pressure ranges: the low-pressure range (10 mPa to 1 Pa); the mid-pressure range (1–100 Pa); and the high-pressure range (100 Pa to 100 kPa).

3.1. Low-pressure range

Below 1 Pa the performance of the sensors is determined by the resolution of the sensors. Usually the resolution is defined as the pressure change leading to a change in output signal equal to the electrical noise of the sensor. For our sensors, which have time constants of the order of 0.1 s (van Herwaarden 1987, pp 44–9, 131–2), the 0–1 Hz band must be used to evaluate the noise. This noise is dominated by the thermal noise of the thermopile resistance, and is of the order of 10–50 nV. With a sensitivity of typically 1–5 mV Pa⁻¹ this results in a resolution of the order of 10 μPa.

However, the resolution we find in this way is not very useful for measurements on a longer term (minutes). In that case the short-term instability of the zero-pressure offset of the sensors is a much more significant source of uncertainty. Any unpredictable change in the offset leads to uncertainty with respect to the pressure indication. An impression of the short-term offset instability has been obtained by measuring three cantilever-beam sensors during longer periods of time. The short-term instability of the offset has been found to be approximately ±0.01%. This is even slightly better than the inaccuracy of ±0.02% of the digital voltmeter used to measure the electrical signals. On the longer term the instability has been found to be approximately one order of magnitude higher: ±0.1%. For a device with a low-pressure sensitivity of 1% change in output signal (normalised to the zero-pressure offset) per pascal pressure change, this implies that, during an experiment or a process, the zero pressure of the device can be predicted to within typically ±10 mPa. On the longer term (months) the uncertainty is of the order of ±100 mPa, so long as the offset is not measured again.

For measurement during an extended period of time (minutes and longer) the short-term instability of the zero-

pressure offset thus determines the performance of the sensors below 1 Pa.

3.2. Mid-pressure range

In the mid-pressure range the errors induced by the instability of the offset fall below 1%. This implies that errors larger than 1% are caused by the limitations of the sensors and of the theoretical models. The prediction errors between 1 and 100 Pa have been determined for various sensors and were found to be maximally 2–3%, that is, the difference between the predicted pressure and the calibration pressure is maximally 2–3% of the calibration pressure. This is in accordance with the expectations based on the repeatability of the characteristic parameters, which is of the order of ±1%. In figures 4 and 5 typical experimental results are shown for cantilever-beam sensors with nitrogen as the test gas, as the normalised decrease defined by equation (4). The parameters shown in the figures have been used together with the sensor output and equation (4) to predict the calibration pressures. Figure 4 shows the performance of sensor 455–82, which has a 6.4 mm long cantilever beam. Note that from 0.2 to 50 Pa the prediction errors, the inaccuracies with which the sensor predicts the calibration pressures, are below 1% (10⁻² on the scale of the right axis). In figure 5 the results for sensor 390–316 are shown, which has a 3.7 mm long cantilever beam. The performance of this sensor is practically identical to that of sensor 455–82, even though its low-pressure sensitivity is much lower, only 0.5% Pa⁻¹, against 1.7% Pa⁻¹ for sensor 455–82.

Because in figures 4 to 7 the deviation from the zero-pressure signal is shown, normalised to the zero-pressure offset, the instability of the offset does not show in these figures.

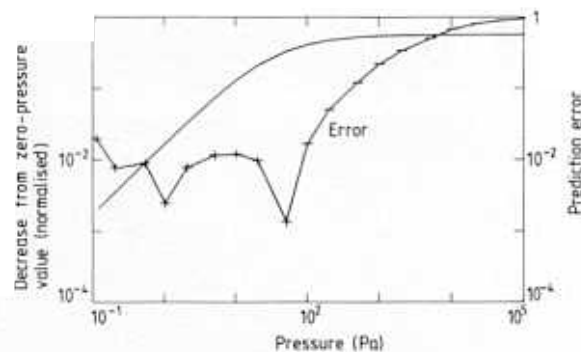


Figure 4. Experimental results and prediction errors of cantilever beam sensor 455-82, for nitrogen. $\frac{1}{3}G_0R_{22}L^2 = 0.0171$, $P_{11} = 51.7 \text{ Pa}$, $P_{12} = 154 \text{ Pa}$

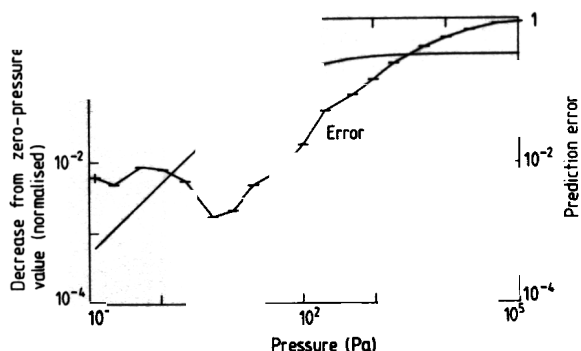


Figure 5. Experimental results and prediction errors of cantilever beam sensor 390-316, for nitrogen. $\frac{1}{3}G_0R_{31}L^2 = 0.00517$, $P_{11} = 52.1 \text{ Pa}$, $P_{12} = 146 \text{ Pa}$

3.3. High-pressure range

At high pressures (>100 Pa) the transition effect and the non-linearity of the cantilever-beam sensors lead to increasing prediction errors. All thermal vacuum sensors suffer from these effects, leading to a high-pressure as well as to a low-pressure limit. We will consider here a so-called *coarse-measurement range*, where the prediction errors lie between 10 and 30%. In applications where—at high pressures—a reliable indication of the magnitude of the pressure is adequate the coarse-measurement range is useful. The coarse-measurement ranges are of the order of 1–5 kPa for argon and nitrogen, and of the order of 5–20 kPa for helium.

For the cantilever-beam sensors 455-82 and 390-316 the coarse-measurement ranges for nitrogen can be seen in figures 4 and 5. Because of their constant-power measurement mode these sensors exhibit large saturation effects at higher pressures, since the temperature of the tip of the beam cannot be cooled to below ambient temperature. This causes a swift increase of the prediction errors above 100 Pa.

In figure 6 the results for sensor 390-316R are shown. This is the same sensor as sensor 390-316, of which the performance is shown in figure 5, except that a so-called roof is put on top of the sensor chip. A roof is a heat sink very close to the hot area of the sensor leading to a high value of the transition pressure and thus improving the high-pressure performance (van Herwaarden 1987 pp 91, 125–31). The increase in the transition pressures is shown by the change in parameters listed in figures 5 and 6 (the roof also slightly decreases the low-pressure sensitivity as is indicated by the change in the factor $\frac{1}{3}G_0R_sL^2$). The result is a significant decrease in the prediction errors at high pressures. The so-called coarse-measurement range for nitrogen is now shifted up from 1–5 kPa to 20–20 kPa (note that at 50 kPa the prediction error rises above 100%, though).

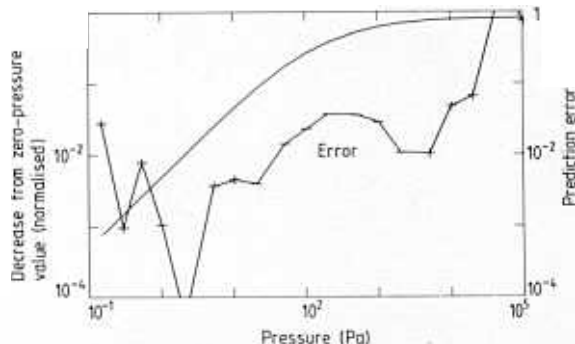


Figure 6. Experimental results and prediction errors of cantilever-beam sensor 390-316R (with roof to improve the high-pressure performance), for nitrogen. $\frac{1}{3}G_0R_sL^2 = 0.00484$, $P_{11} = 157$ Pa, $P_{12} = 4227$ Pa.

In figure 7 the results for the floating-membrane sensor 454-81R are depicted. This sensor has also been equipped with a roof, leading to high transition pressures. Because of the different operational mode of this sensor, a constant-temperature mode rather than the constant-power mode of the cantilever-beam sensors, no saturation effects occur at high pressures, and satisfactory operation up to much higher pressures is possible (Steckelmacher 1973). This is reflected in the low prediction errors up to atmospheric pressure (100 kPa), compared with the cantilever-beam sensor 390-316R with roof. A very high coarse-measurement range results, with a 100 kPa upper bound.

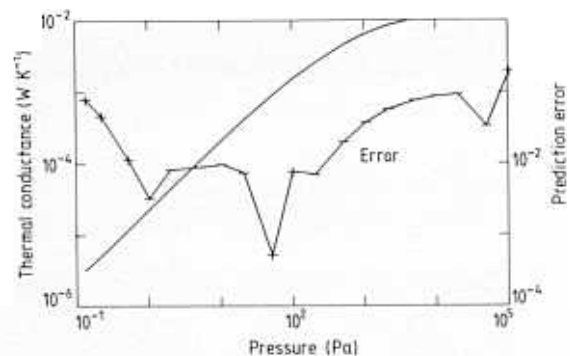


Figure 7. Experimental results and prediction errors of floating-membrane sensor 454-81R (with roof to improve the high-pressure performance), for nitrogen. $\frac{1}{3}G_0 = 1.8452$ Wm⁻²K⁻¹Pa⁻¹, $P_{11} = 89$ Pa, $P_{12} = 1054$ Pa.

4. Comparison with conventional Pirani gauges

To give an impression of how the performance of the sensors must be judged we will make a comparison with the results of the experiments on Pirani gauges carried out by Poulter *et al* (1980). They have investigated the reproducibility of the performance of Pirani gauges. These were tested between 0.133 Pa and 1.33 kPa with nitrogen and argon as test gases.

At the test pressures a maximum change in the pressure indication by the gauges under test of 1.6% for nitrogen and 1.8% for argon between successive experiments was found. The definition of Poulter *et al* regarding the changes in the pressure indication makes these changes similar to our prediction errors. For pressures between 0.2 and 100 Pa the prediction errors are maximally 2–3%. This indicates that between 0.2 and 100 Pa the performance of our sensors is comparable with that of the Pirani gauges. A comparison at 1 kPa is difficult to achieve. A significant difference between the experiments exists in that the atmospheric-pressure output of the Pirani gauges was adjusted to the proper value at the beginning of the measurements.

The temperature coefficient of the offset of the Pirani gauges, approximately 0.5% K⁻¹, is one order of magnitude worse than that of the integrated sensors, which has, for a number of sensors, been measured at between 20 and 30 °C and has been found to be of the order of $\pm 0.05\%$ K⁻¹. The temperature coefficient of the sensitivity of the Pirani gauges is also of the order of 0.5% K⁻¹. For the integrated devices no measurement results are available, but a somewhat lower temperature coefficient of 0.2% K⁻¹ is estimated. The long-term (3 months) instability of the zero-pressure output was 7% for high-pressure and 20% for low-pressure Pirani gauges. This compares unfavourably with the 0.1% for the integrated devices but usually the long-term offset instability is of lesser importance.

5. Conclusion

The integrated-thermopile vacuum sensors can successfully measure pressure on the basis of a simple model with three parameters: low-pressure sensitivity and two transition pressures. This makes it possible to correct for gas type and ambient temperature by adapting the parameters. The offset repeatability of the sensors of $\pm 0.01\%$ implies a zero-pressure repeatability of the order of 10 mPa. The optimum range of the sensors lies between 1 and 100 Pa, and in this range the errors in the pressure measurement are below 2–3%. At higher pressures the errors increase leading to an upper limit above which the usefulness of the sensors

Performance of integrated thermopile vacuum sensors

decreases. Depending on the gas type and the sensor structure the upper limit ranges from 2 to 100 kPa. A comparison with conventional Pirani gauges suggests that the performance of the first prototypes of integrated vacuum sensors successfully compares with that of fully developed types of conventional Pirani gauges tested under primary-standards laboratory conditions.

Acknowledgments

The authors would like to thank the staff of the Departmental IC Workshop for manufacturing the devices. They also wish to thank Mr E Smit, Ir P K Nauta and Professor S Middelhoek for their helpful suggestions during the project. These investigations, included in the program of the Foundation for Fundamental Research on Matter (FOM), have been supported in part by the Netherlands Technology Foundation (STW).

References

- Dushman S 1962 *Scientific Foundations of Vacuum Technique* 2nd edn (New York: Wiley) pp 49–53
- van Herwaarden A W 1987 Thermal vacuum sensors based on integrated silicon thermopiles
PhD Thesis Delft University of Technology, The Netherlands
- van Herwaarden A W and Sarro P M 1987 Double beam integrated thermal vacuum sensor
J. Vac. Sci. Technol. A **5** 2454–7
- van Herwaarden A W and Sarro P M 1988 Floating-membrane thermal vacuum sensor
Sensors and Actuators **14** 259–68
- Poulter K F, Rodgers M-J and Ashcroft K W 1980 Reproducibility of the performance of Pirani gauges
J. Vac. Sci. Technol. **17** 638–41
- Sarro P M and van Herwaarden A W 1986 Silicon cantilever beams fabricated by electrochemically controlled etching for sensor applications
J. Electrochem. Soc. **133** 1724–9
- Steckelmacher W 1973 The high pressure sensitivity extension of thermal conductivity gauges
Vacuum **23** 307–11